Student-T and Beyond: Practical Tools for Multiple-Scattering BSDFs with General NDFs

Eugene d'Eon
NVIDIA
SIGGRAPH 2023 Talks

May 26, 2023

1 Summary

In this supplemental PDF we:

- Provide expanded plots and description of our comparison of ST rough dielectric BSDFs to measured data (subsection 2.1)
- Give a detailed derivation of the Beckmann-superposition vNDF sampling scheme for the Student-T NDF (section 2)
- Discuss our null-collision algorithm for sampling and evaluating multiple scattering from rough and porous generalized Smith surfaces with NDFs extending to the full sphere, together with some new parametric NDFs and their properties (section 3)
- Discuss details of our BSDF interface that permits easily implementation of new null and shape invariant NDFs (section 4)
- Discuss several results that were created using the above tools (section 5)

2 Student-T NDF: New Sampling and Motivation

2.1 ST comparisons to Rough Glass

The GGX NDF (equivalent to the Trowbridge-Reitz NDF) was made popular in graphics by Walter et al. (2007) after using it to approximate the behaviour of *ground glass*, noting that Beckmann's NDF was a less accurate choice. In the same work, it was observed that several glass samples (etched and frosted) appeared to exhibit a behaviour somewhat between GGX and Beckmann, with neither constituting an optimal choice.

The Student-T (ST) NDF (Ribardière et al., 2017) was later introduced and conveniently interpolates between Beckmann ($\gamma = \infty$) and GGX ($\gamma = 2$) via its dependence on an additional shape parameter $\gamma > 3/2$. The primary reasons for proposing this NDF were convenient mathematical properties that are required for its efficient use (such as closed-form shadowing/masking factors). To the best of our knowledge, ST BSDFs have not been compared to measured data in order to determine if ST is indeed a good physically-motivated choice for interpolating between Beckmann and GGX.

In this section, we revisit the original data from Walter et al. (2007) and compare predictions of the ST microfacet BSDFs to the measurements for the ground, etched, and frosted glass samples. In Figures 1 - 3, we plot each measurement from Walter et al. (2007) and compare to Beckmann, GGX and two ST BSDFs: one where $\gamma = 3$ is fixed and one where γ is free to vary for that sample. Our plots differ from those of Walter et al. (2007) by plotting $\sqrt{L}$ to provide an approximate gamma correction, which allows closer inspection of the errors in the darker regions of the measurements. In the case of frosted and etched glass, we see that the ST NDF not only outperforms GGX and Beckmann, but in fact matches the measurements of both samples as accurately (or more) than GGX matches the ground glass measurements. From this we conclude that ST is a very strong choice for a two-parameter model that can blend between the statistics of Beckmann and GGX surfaces. Renders of rough glass using these settings and comparisons to Walter's original GGX and Beckmann fittings are provided in the supplemental images folder.

To put the ST NDF on equal computational footing to Beckmann and GGX, in the next section we derive vNDF sampling, which is required for low-variance single-scattering sampling, as well as reference-quality random walk multiple-scattering (required to avoid large energy loss at high roughnesses as seen in (Ribardière et al., 2017, Fig.7)).

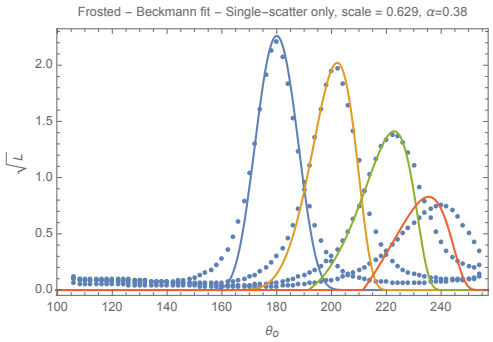

(a) slightly tweaked 2007 fit with Beckmann

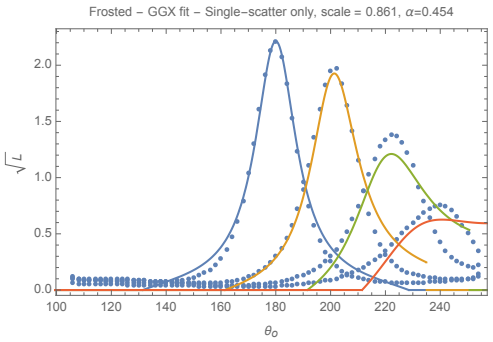

(b) 2007 fit with GGX

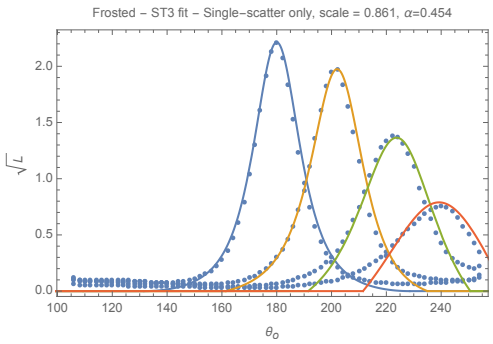

(c) Student-T with $\gamma = 3$

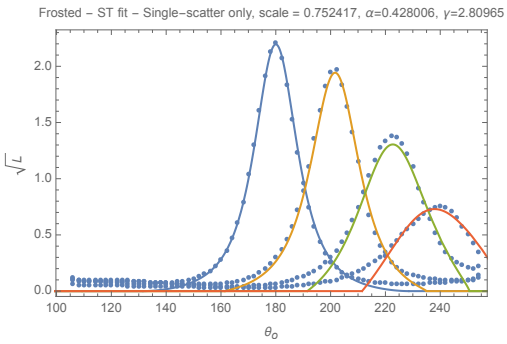

(d) general Student-T fit

Figure 1: Frosted glass: note how for the two most grazing measurements in each plot (peaking around 220 and 240 degrees) the ST fits (c-d) are more accurate than previous models (a-b). Note also the improved accuracy of ST for the normal (180) profile for low intensities.

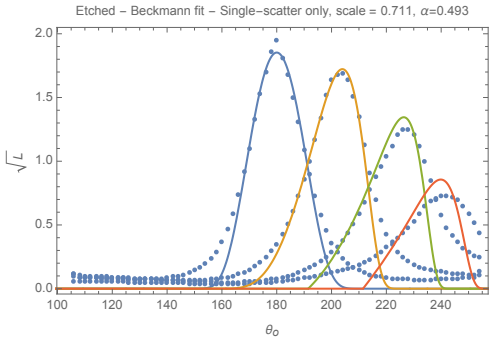

(a) 2007 fit with Beckmann

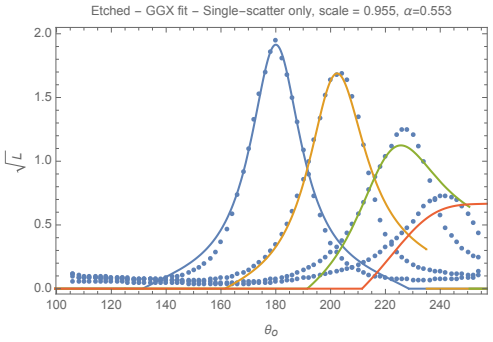

(b) 2007 fit with GGX

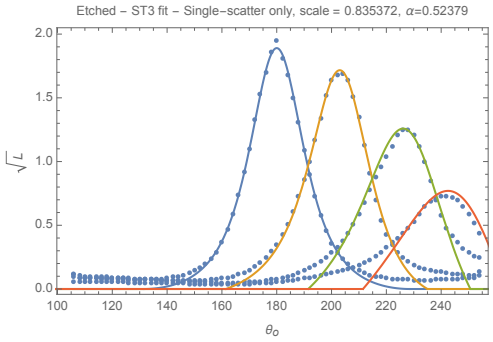

(c) Student-T with $\gamma = 3$

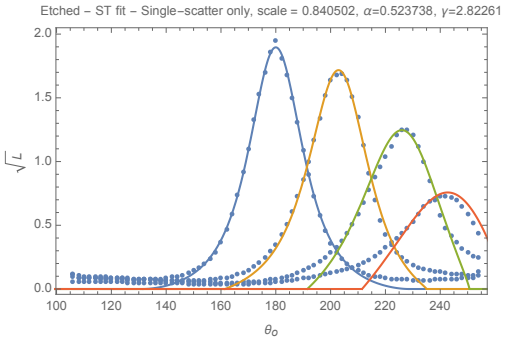

(d) general Student-T fit

Figure 2: Etched glass: note a similar improvement of ST over Beckmann or GGX for both low intensities and for the more grazing (220, 240 peaked) profiles.

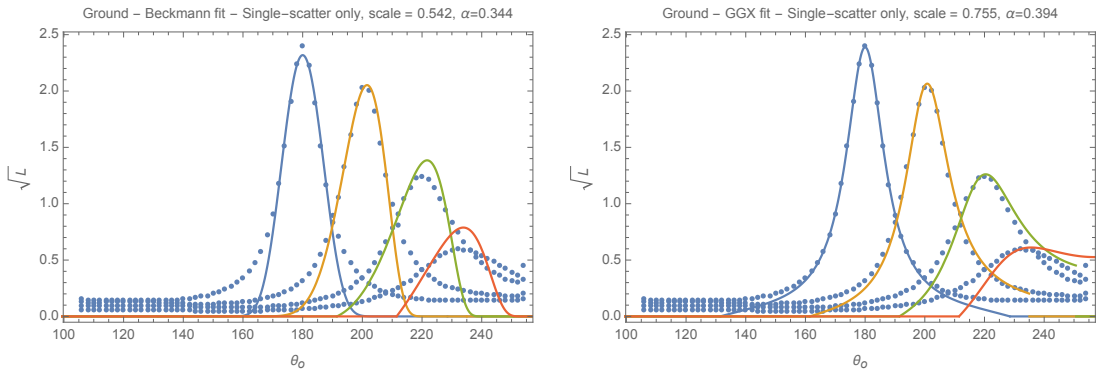

(a) 2007 fit with Beckmann

(b) 2007 fit with GGX

(c) Student-T with $\gamma = 3$

(d) general Student-T fit

Figure 3: Ground glass: in this case the GGX distribution (b), which was motivated by this exact physical sample, performs best and is not improved upon by Student-T.

2.2 Review

Before deriving our ST sampling procedure, we begin with some necessary review. With notation $u = \cos\theta_m$, the Beckmann NDF with roughness α is (Blinn, 1977)

$$D^{\mathrm{B}}(u,\alpha) = \frac{e^{-\frac{\frac{1}{u^2}-1}{\alpha^2}}}{\pi\alpha^2 u^4}\Theta(u), \tag{1}$$

where $\Theta(u)$ is Heaviside's function. The GGX NDF is

$$D^{\mathrm{GGX}}(u,\alpha) = \frac{\alpha^2}{\pi u^4\left(\alpha^2 + \frac{1}{u^2} - 1\right)^2}\Theta(u) \tag{2}$$

and the student-T NDF is

$$D^{\mathrm{ST}}(u,\alpha,\gamma) = \frac{(\gamma-1)^\gamma \alpha^{2\gamma-2}\left(\alpha^2(\gamma-1) + \frac{1}{u^2} - 1\right)^{-\gamma}}{\pi u^4}\Theta(u), \quad \gamma > \frac{3}{2}. \tag{3}$$

The corresponding slope distribution is

$$P_{22}^{\mathrm{ST}}(p,q,\alpha,\gamma) = \frac{(\gamma-1)^\gamma \alpha^{2\gamma-2}\left(\alpha^2(\gamma-1) + p^2 + q^2\right)^{-\gamma}}{\pi} \tag{4}$$

with marginal slope distribution

$$P_2^{\mathrm{ST}}(p,\alpha,\gamma) = \frac{(\gamma-1)^\gamma \alpha^{2\gamma-2}\Gamma\left(\gamma-\frac{1}{2}\right)\left(\alpha^2(\gamma-1) + p^2\right)^{\frac{1}{2}-\gamma}}{\sqrt{\pi}\Gamma(\gamma)} \tag{5}$$

The scattering cross-section is

$$\sigma^{\mathrm{ST}}(u,\alpha,\gamma) = \frac{u^2\Gamma\left(\gamma-\frac{1}{2}\right)\,{}_2F_1\left(\frac{1}{2},\gamma-\frac{1}{2};\frac{3}{2};\frac{u^2}{(u^2-1)\alpha^2(\gamma-1)}\right)}{\sqrt{\pi}\alpha\Gamma(\gamma-1)\sqrt{(\gamma-1)\,(1-u^2)}} + \frac{\alpha\Gamma\left(\gamma-\frac{3}{2}\right)\sqrt{(\gamma-1)\,(1-u^2)}\left(1-\frac{u^2}{\alpha^2(\gamma-1)(u^2-1)}\right)^{\frac{3}{2}-\gamma}}{2\sqrt{\pi}\Gamma(\gamma-1)} + \frac{u}{2}. \quad (6)$$

2.3 Student-T as a superposition of Beckmann surfaces

The key insight to our method is to note that the ST NDF can be expressed as a gamma-superposition of Beckmann NDFs:

$$D^{\mathrm{ST}}(u,\alpha,\gamma) = \int_0^\infty \frac{e^{-m}m^{\gamma-2}}{\Gamma(\gamma-1)} D^{\mathrm{B}}\left(u,\alpha\sqrt{\frac{\gamma-1}{m}}\right)\mathrm{d}m. \quad (7)$$

We will use the method of continuous decomposition ((Butler, 1954, p.254), (d'Eon, 2022, Sec. 70.3.3)) for sampling non-uniform random variates, where a target distribution is expressed as a superposition of another parametric distribution, for which a sampling procedure is known. Here the parameter $m > 0$ indexes the superposition, and for each m the roughness of the corresponding Beckmann distribution in the mixture is $\alpha\sqrt{(\gamma-1)/m}$.

2.4 Sampling the visible distribution of normals

For a ray arriving straight down along the surface normal, we could sample the ST vNDF in a two stage procedure using Equation 7 to first sample m from the gamma distribution

$$\frac{e^{-m}m^{\gamma-2}}{\Gamma(\gamma-1)} \quad (8)$$

(using Marsaglia's method or C++ 11 code) and then sample the Beckmann NDF with roughness $\alpha_{\mathrm{B}} = \alpha\sqrt{(\gamma-1)/m}$. However, when the incoming direction ω_i is not along the normal, we require a different distribution, due to how the various Beckmann distributions in the continuous mixture self shadow each other. We can find this distribution by repeating the slope-space derivation of Heitz and d'Eon (2014), but with Equation 7 as the NDF. We find that we need to sample slope p from the marginal slope distribution (Equation 5)

$$\int_{-\infty}^{u/\sqrt{1-u^2}} P_2^{\mathrm{ST}}(p,\alpha,\gamma)(u-p\sqrt{1-u^2})\mathrm{d}p, \quad (9)$$

which we expand using the gamma superposition (Equation 7) to find

$$P_2^{\mathrm{ST}}(p,\alpha,\gamma) = \int_0^\infty \frac{m^{\gamma-\frac{3}{2}}e^{m\left(-\frac{p^2}{\alpha^2(\gamma-1)}-1\right)}}{\sqrt{\pi}\alpha\sqrt{\gamma-1}\Gamma(\gamma-1)}\mathrm{d}m. \quad (10)$$

Combining the last two equations, and integrating over p, we are left with a distribution over m. Using stretch invariance, we can solve the problem for roughness $\alpha = 1$ and linearly scale the sampled Beckmann roughness by α. We find for $\alpha = 1$,

$$f(m,u) = \int_{-\infty}^{\frac{u}{\sqrt{1-u^2}}} \frac{m^{\gamma-\frac{3}{2}}e^{m\left(-\frac{p^2}{\gamma-1}-1\right)}}{\sqrt{\pi}\sqrt{\gamma-1}\Gamma(\gamma-1)}\left(u-p\sqrt{1-u^2}\right)\mathrm{d}p = \frac{e^{-m}um^{\gamma-2}\mathrm{erf}\left(u\sqrt{-\frac{m}{(\gamma-1)(u^2-1)}}\right)}{2\Gamma(\gamma-1)} + \frac{m^{\gamma-\frac{5}{2}}\sqrt{-((\gamma-1)(u^2-1))}e^{m\left(\frac{u^2}{(\gamma-1)(u^2-1)}-1\right)}}{2\sqrt{\pi}\Gamma(\gamma-1)} + \frac{e^{-m}um^{\gamma-2}}{2\Gamma(\gamma-1)}. \quad (11)$$

We want to sample from this distribution, so we must normalize it. The normalization

$$\hat{f}(m,u) \equiv \frac{f(m,u)}{\int_0^\infty f(m,u)\mathrm{d}m} \quad (12)$$

gives the probability density for the Beckmann NDF indexed by m to contribute to the ST vNDF for a ray arriving along cosine u. Its normalization is simply the cross section for the ST NDF (Equation 6),

$$\int_0^\infty f(m,u)\mathrm{d}m = \sigma(u) = (1+\Lambda(u))u. \quad (13)$$

If we can sample m from $\hat{f}(m,u)$ given u, then we can then sample the Beckmann vNDF with roughness $\alpha_B = \alpha\sqrt{(\gamma-1)/m}$ and we have sampled the ST vNDF.

2.5 Sampling m from the upper hemisphere

For $u > 0$, the density f in Equation 11 is a sum of three non-negative densities, each involving gamma distributions. We can sample the sum by discrete decomposition (Everett and Cashwell, 1983, C3. p.55). The term involving erf can be sampled using a rejection procedure. We first decompose $\hat{f}$ into three terms

$$\hat{f}(m,u) = p_1(u)f_1(m,u) + p_2(u)f_2(m,u) + p_3(u)f_3(m,u) \tag{14}$$

where f_i are normalized densities over $m \in [0,\infty]$. We define

$$\begin{aligned}
f_1(m,u) &= \frac{b^{\frac{3}{2}-\gamma} e^{-\frac{m}{b}} m^{\gamma-\frac{5}{2}}}{\Gamma\left(\gamma-\frac{3}{2}\right)},\\
f_2(m,u) &= \frac{e^{-m} m^{\gamma-2}}{\Gamma(\gamma-1)},\\
f_3(m,u) &= \frac{\sqrt{\pi}\sqrt{\gamma-1}e^{-m}m^{\gamma-\frac{5}{2}}\sqrt{(\gamma-1)m}\,\mathrm{erf}\left(u\sqrt{-\frac{m}{(\gamma-1)(u^2-1)}}\right)}{2u\Gamma\left(\gamma-\frac{1}{2}\right)\sqrt{\frac{1-\gamma}{u^2-1}}\,{}_2F_1\left(\frac{1}{2},\gamma-\frac{1}{2};\frac{3}{2};\frac{u^2}{(u^2-1)(\gamma-1)}\right)},\\
b &\equiv \frac{1}{1-\frac{u^2}{(\gamma-1)(u^2-1)}}.
\end{aligned}$$

We find (by integrating each over $m > 0$ in Mathematica) that the discrete selection probabilities for the three densities are

$$p_1(u) = \frac{(\gamma-1)^{3/2}\sqrt{1-u^2}\,\Gamma\left(\gamma-\frac{3}{2}\right)\left(1-\frac{u^2}{(\gamma-1)\left(u^2-1\right)}\right)^{\frac{3}{2}-\gamma}}{2\sqrt{\pi}\left(\frac{\Gamma\left(\gamma-\frac{1}{2}\right)\sqrt{\frac{\gamma-\left((\gamma-2)u^2\right)-1}{\gamma-1}}\left(\left(-2\gamma^2+5\gamma-3\right)u^2\sqrt{\frac{u^2-1}{-\gamma+(\gamma-2)u^2+1}}\,{}_2F_1\left(\frac{1}{2},\gamma-\frac{1}{2};\frac{3}{2};\frac{u^2}{\left(u^2-1\right)(\gamma-1)}\right)+(\gamma-1)^{\gamma+\frac{1}{2}}\left(u^2-1\right)\left(\frac{u^2-1}{-\gamma+(\gamma-2)u^2+1}\right)^{\gamma-1}\right)}{\sqrt{\pi}(2\gamma-3)\left(u^2-1\right)}+\frac{u\Gamma(\gamma)}{2}\right)} \tag{15}$$

$$p_2(u) = \frac{(\gamma-1)u\Gamma(\gamma-1)}{2\Gamma\left(\gamma-\frac{1}{2}\right)\sqrt{\left(\frac{1}{\gamma-1}-1\right)u^2+1}\left(\left((5-2\gamma)\gamma-3\right)u^2\sqrt{\frac{u^2-1}{-\gamma+(\gamma-2)u^2+1}}\,{}_2F_1\left(\frac{1}{2},\gamma-\frac{1}{2};\frac{3}{2};\frac{u^2}{\left(u^2-1\right)(\gamma-1)}\right)+\sqrt{\gamma-1}\left(-\gamma+(\gamma-2)u^2+1\right)\left(\frac{u^2}{-\gamma+(\gamma-2)u^2+1}+1\right)^{\gamma}\right)}{\sqrt{\pi}(2\gamma-3)\left(u^2-1\right)}+u\Gamma(\gamma)} \tag{16}$$

$$p_3(u) = 1 - p_1(u) - p_2(u). \tag{17}$$

The final procedure for sampling the visible distribution of normals for the ST NDF for an incident direction pointing down towards the surface with cosine $0 < u < 1$ is to first select a lobe f_i using discrete probabilities $\{p_1(u), p_2(u), p_3(u)\}$, then sample m from the corresponding density $\{f_1(m,u), f_2(m,u), f_3(m,u)\}$, and finally sample the Beckmann vNDF with roughness $\alpha_B = \alpha\sqrt{(\gamma-1)/m}$.

Densities f_1 and f_2 are gamma distributions and can be directly sampled using C++ 11 methods. Specifically, f_1 is a gamma distribution with shape parameter $a = \gamma - \frac{3}{2}$ and scale parameter b defined above. f_2 is a gamma distribution with shape parameter $a = \gamma - 1$ and shape parameter $b = 1$. We finally note that f_3 is a gamma distribution with shape parameter $a = \gamma - 1$ and scale $b = 1$ that is modulated by the function $\mathrm{erf}\left(u\sqrt{-\frac{m}{(\gamma-1)(u^2-1)}}\right)$, which can be sampling using rejection by repeatedly sampling m from the corresponding gamma distribution and rejecting and trying again each time $\xi_i < \mathrm{erf}\left(u\sqrt{-\frac{m}{(\gamma-1)(u^2-1)}}\right)$, where $\xi_i \in [0,1]$ are uniform variates. We observed the expected number of gamma random variates required to sample the vNDF is 1.2, so the rejection of f_3 happens infrequently. We remark that for $\gamma \in \{2,3,4\}$ it is possible to exactly sample f_3 using a fixed number of random variates.

The probabilities p_1 and p_2 are inconvenient functions of cosine u and include the hypergeometric function 2F1. For these reasons, we derived (using TuringBot) approximate equations (provided in the supplemental code) for each, which we observed to work very well in practice.

2.6 Upwelling case

The down-welling case is sufficient for BSDF sampling the single-scattering portion of the rough surface. However, for a full multiple-scatter random walk, we also need to handle vNDF sampling for up-welling

rays ($-1 < u < 0$) (Heitz et al., 2016). Unfortunately, this requires a different sampling procedure because the three terms in the m-sampling density $f(m,u)$ are no longer non-negative, excluding the possibility of sampling by discrete decomposition.

We propose an approximate solution using generalized gamma distributions. We observed that the target distribution $f(m, u < 0)$ is well approximated by a generalized gamma distribution with three parameters a, b, and c, with probability density

$$p(m) = \begin{cases} \frac{c e^{-\left(\frac{m}{b}\right)^c} \left(\frac{m}{b}\right)^{ac-1}}{b\Gamma(a)} & m > 0 \\ 0 & \text{True} \end{cases} \tag{18}$$

This distribution can be sampled by sampling a gamma variate x with parameter a and width $b = 1$, and then returning $m = bx^{1/c}$ (Tadikamalla, 1979). We used a fitting procedure (TuringBot) to find the constants a, b, and c, given cosine u and shape γ. We determine b first by requiring that it match the exact first moment of the target distribution,

$$m_1 = \frac{\frac{\Gamma\left(\gamma-\frac{1}{2}\right)\left(\sqrt{\gamma-1}(2\gamma-1)u^2\,{}_2F_1\left(\frac{1}{2},\gamma+\frac{1}{2};\frac{3}{2};\frac{u^2}{(u^2-1)(\gamma-1)}\right)+(\gamma-1)\sqrt{(u^2-1)(-\gamma+(\gamma-2)u^2+1)}\left(1-\frac{u^2}{(\gamma-1)(u^2-1)}\right)^{-\gamma}\right)}{\sqrt{\pi-\pi u^2}\Gamma(\gamma)} + (\gamma-1)u}{2\sigma(u)}. \tag{19}$$

Then constant b is selected to ensure this same moment in the approximation, giving

$$b = \frac{m_1\Gamma(a)}{\Gamma\left(a+\frac{1}{c}\right)}. \tag{20}$$

Our fitting experiments found approximations for a and c,

$$a = \gamma - \frac{0.0655156(u+0.0442664)}{\cos(\gamma+0.633638)+1.20697} - 1.49293 \tag{21}$$

$$c = \frac{u+0.0138041}{0.516877\gamma^2 - u - \sinh^{-1}(u) - 0.850096} + 1.00448. \tag{22}$$

2.7 Discussion

We have tested the above sampling procedure and found excellent agreement compared to a sampling of the ST vNDF using a null collision (rejection) procedure and verified that the supplemental code produces close results to GGX and Beckmann BSDF values when γ is appropriately set.

This sampling scheme has several limitations, such as its use of a theoretically unbounded number of random variates per sample, as well as the requirement for gamma variates. In practice, we observed the rejection scheme required for the down-welling case to happen about 20% of the time. A further limitation is that both the superposition sampling and rejection will hinder the application of low discrepancy sampling schemes.

3 A Null-Scattering Formulation of Rough Surface Scattering

In this section we derive a new Monte Carlo procedure for stochastically evaluating and sampling Smith microfacet BRDFs. This approach is motivated by two goals: 1) to allow quick and easy addition of new NDFs to a material system, and 2) to expand on the proposal of Dupuy et al. (2016) to formulate a Smith theory of microfacet scattering for highly rough materials where some microfacets face into the downward hemisphere, thereby violating the *height-field assumption* of the standard microfacet theory (Smith, 1967). Smith's theory is a powerful general method for modeling surface scattering and supports anisotropy (Heitz, 2014), importance sampling (Heitz and d'Eon, 2014) and multiple-scattering (Heitz et al., 2016) for many surface statistics (Walter et al., 2007; Ribardière et al., 2017). However, the height-field assumption is not universally appropriate, and deriving Lambda functions and vNDF sampling procedures is not always possible.

Dupuy et al. (2016) describe a generalization of the Smith theory for a volume where the NDF extends to support the full sphere of directions. This was accomplished by noting that all Smith heightfield volumetric models correspond exactly to a generalization of a uniform anisotropic/microflake (Jakob et al., 2010) half space of spatially-independent scattering particles/flakes. The total anisotropic macroscopic cross section $\sigma_t(\omega)$ governing this volume was found to be the normalization factor of the distribution of visible normals for the given NDF $D(\omega)$ of the material, via the relationship (Dupuy et al., 2016, Eq.(6))

$$D_{vis}(\omega_m, \omega) = \frac{\langle -\omega_m, \omega\rangle D(\omega_m)}{\sigma_t(\omega)}, \tag{23}$$

where $\langle \omega_1, \omega_2 \rangle \geq 0$ is a clamped dot product. The volumetric equivalence in Equation 23 immediately and uniquely determines the required random walk: given any NDF $D(\omega_m) \geq 0$ the free-path length distribution for sampling random walks in the volume along direction ω is then

$$p(s;\omega) = \sigma_t(\omega) e^{-\sigma_t(\omega)s}. \tag{24}$$

After each collision (moving in direction ω), a microfacet normal ω_m is then sampled from the normalized distribution $D_{vis}(\omega_m, \omega)$ and the BSDF of that microfacet is sampled to determine the new direction. This process is continued until the ray escapes the half space. However, this requires accurate numerical evaluation of σ_t and importance sampling of $D_{vis}(\omega_m, \omega)$.

No specific NDF or related procedure for sampling distances and visible normals in such a medium was presented by Dupuy et al. (2016). In a followup paper (d'Eon, 2016) it was shown that the cross section for the von-Mises Fisher (vMF) distribution was complicated, and no sampling procedure for the related distribution $D_{vis}(\omega_m, \omega)$ has been found. To the best of our knowledge, no practical numerical scheme for evaluating a non-uniform full-sphere NDF BRDF has been presented.

In this talk, we show how an approach inspired from Woodcock/delta tracking for sampling distances in inhomogeneous volumes (Novák et al., 2018) can stochastically evaluate any generalized Smith model given only the NDF and its majorant as input, requiring no additional derivations. Where delta-tracking in inhomogeneous volumes *spatially* homogenizes the cross section $\sigma_t(x)$, we use an analagous procedure to homogenize the cross section *in the angular domain* $\sigma_t(\omega)$ (it is already spatially homogeneous). This is achieved by introducing just enough virtual microflakes to homogenize the cross section to be a constant over the sphere of microfacet normal directions. Collisions with the new medium result in some (directionally-dependent) portion of those collisions to be virtual/null, resulting in the rejection of these collisions, with the random walk continuing in the same direction as if the null flake was never present.

3.1 The Algorithm

We consider a homogeneous half space of scattering and absorbing particles/flakes. Spatial homogeneity implies no dependence on position for the cross section $\sigma_t(\omega)$, but the angular dependence via direction ω is required to exhibit the correlations of surface scattering, with (in general) asymmetry $\sigma_t(\omega) \neq \sigma_t(-\omega)$ (Dupuy et al., 2016). To sample the microfacet BRDF, given incoming direction ω_i and general NDF, possibly defined over the full sphere, we use the following algorithm:

- Given an NDF $D(\omega_m) \geq 0$, we define the constant majorant NDF $\bar{D}(\omega_m) \geq D(\omega_m)$ whose value is the maximum that the NDF D takes on (typically the value straight up along the macrosurface normal).
- We stochastically evaluate the microfacet BRDF by sampling a random walk in the half space, using the homogeneized volumetric Smith model Dupuy et al. (2016). The walk begins at the boundary along with initial direction $\omega = -\omega_i$, where ω_i is the common BRDF notation of a vector pointing *away* from the surface.
- We sample all collisions in the medium using null scattering. Specifically, we collide with the angularly homogeneized distribution of microfacets (with NDF $\bar{D}(\omega_m)$). Combining Equation 23 with the uniformity of the NDF results in σ_t is being a constant. Without loss of generality, since we are computing a BRDF with no lateral displacement (sometimes known as "position-free simulation" Guo et al. (2018), even though the depth-tracking is necessary), and because the surface is expanded into a half space, we can assume $\sigma_t = 1$.
- While no actual particles are traced against, the following geometrical procedure illustrates the core sampling idea. For each sampled collision (real or ficticious), we consider a small spherical particle with the pair of NDF values (real and ficticious) mapped to its surface (Figure 4). We then consider a uniform field of rays along direction ω intersecting this sphere, and sample from this set of rays uniformly at random (using disk sampling following by rotation to ω and then a ray-sphere intersection test). This produces a microfacet normal ω_m that is the surface normal of the sphere at the intersected location. Using this microfacet normal direction we consider that this sampled collision is *real* with probability $D(\omega_m)/\bar{D}(\omega_m)$ and otherwise ignore the collision and sample a new distance with ω unchanged, analogous to delta tracking in inhomogeneous media (see Figure 4).
- For each real collision, the BSDF of the microfacets is sampled using ω and ω_m to determine the next direction of the random walk.
- Upon exiting the half space, the particle weight (which may deviate from 1 for absorbing microfacets) and direction ω are returned.

This procedure is equivalent to Smith's model in the case that the NDF is restricted to the upper hemisphere. We have verified this via MC simulation for Beckmann and GGX NDFs.

An important property of this algorithm is that it jointly samples free-path-lengths $p(s;\omega)$ and visible normals $D_{vis}(\omega_m)$ in a single step, *without having to know* $\sigma_t(\omega)$. The disk projection of uniform

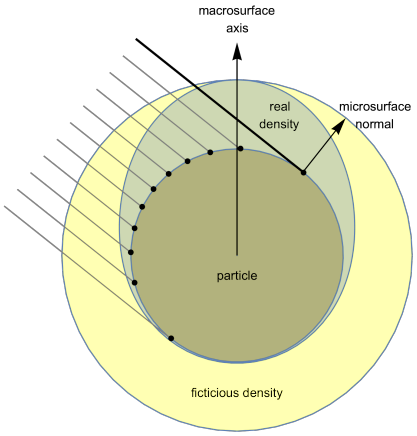

Figure 4: Illustration of our stochastic null-scattering formulation of non-heightfield Smith scattering. We model a rough surface as a homogeneous half space of scattering particles with no spatial correlation. Each time a particle collision is sampled, we select a random ray along the current direction (thick line) from a uniform field of rays that intersect a virtual spherical particle (thin lines). At the intersection point of the sampled ray with the particle (black dots), we consider the amounts of real and ficticious density in the NDF at the sampled microfacet direction. Here the real and ficticious NDFs are plotted parametrically, offset from the particle to illustrate their relative magnitudes. In the illustrated example here (the sampled thick path), roughly 60% of the total density of the uniform majorant NDF in the sampled direction is real, and so the particle is stochastically determined to cause a true collision with probability 60%, and the sampled microfacet normal is used with the BRDF of the microfacet to sample the next direction. This process continues until the path exits the half space, and the final direction and weight of the path are returned.

rays onto the sphere exactly accounts for the geometry term (the clamped dot product) in Equation 23 and the rejection procedure exactly normalizes the true distribution, and by Equation 23 produces the desired exponential mean free path length $\sigma_t(\omega)$ (this follows from properties of Poisson processes, see e.g. Georgiev et al. (2019)).

Another key feature of this algorithm is that only $D(\omega_m)$ is required to implement sample(). This permits adding almost any (bounded) NDF to a renderer.

3.2 Next-Event Estimation

In order to implement eval(), we require the same random walk as in the sample() method, but with NEE at each real collision along outgoing direction ω_o. This requires knowing the extinction in direction ω_o, which depends on the cross section $\sigma(\omega_o)$ of the NDF. In practice, this function is unavailable in closed form for many NDFs. To circumvent this limitation, and simplify the addition of new NDFs to the material library, we use the cross section of the Dirac NDF (described next) as a Green's function and numerically compute $\sigma(\omega_o)$ using a 1D quadrature over the cosine of the microfacet orientations (note that this step of the algorithm is limited to *symmetric* NDFs that depend only on direction cosine u).

3.2.1 The Dirac NDF

The general case of a Dirac ring on the sphere of normal directions with azimuthal symmetry corresponds to a surface where all normals inclined by a common cosine, u_n. This might arise in the case of a surface that is thoroughly pitted by the tip of a hard cone oriented along the mean normal (Figure 5). The Dirac NDF is simply

$$D(u) = \delta(u - u_n), \tag{25}$$

and leads to a piecewise simple expression for the cross-section (d'Eon, 2016)

$$\sigma_\delta(u, u_n) = \begin{cases} 2\pi u u_n & \left(u_n < 0 \wedge u < -\sqrt{1-u_n^2}\right) \vee \left(u_n > 0 \wedge u > \sqrt{1-u_n^2}\right) \\ 2\left(\sqrt{-u_n^2 - u^2 + 1} + u u_n \cos^{-1}\left(-\frac{u u_n}{\sqrt{1-u^2}\sqrt{1-u_n^2}}\right)\right) & u > -\sqrt{1-u_n^2} \wedge u < \sqrt{1-u_n^2} \end{cases}.$$

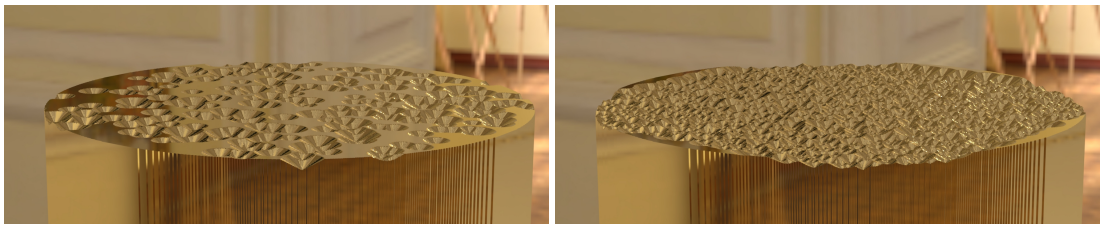

(a) Lightly pitted (b) Thoroughly pitted

Figure 5: A smooth gold surface pitted with a conical tip aligned to the surface normal creates a micro-surface with an isotropic NDF given by a Dirac delta of the cosine of the microfacets to the macrosurface normal.

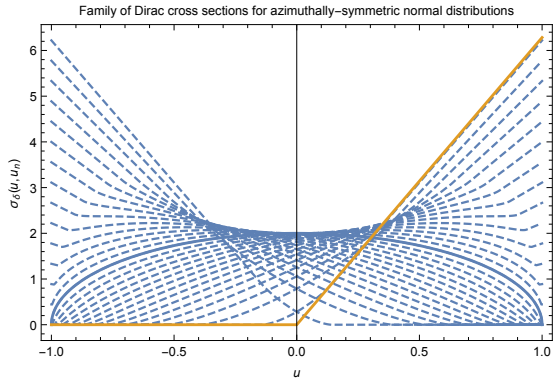

Figure 6: The Dirac-delta cross sections $\sigma_\delta(u, u_n)$ for a variety of u_n form a family of normalized functions blending between $\pi(u + |u|)$ and $2\sqrt{1-u^2}$.

The Dirac NDF cross section can be decomposed into three functions,

$$\sigma_\delta = \sigma_{\delta 1} + \sigma_{\delta 2} + \sigma_{\delta 3} \tag{26}$$

$$\sigma_{\delta 1} = \begin{cases} 2\pi u u_n & u u_n > 0 \\ 0 & else \end{cases} \tag{27}$$

$$\sigma_{\delta 2} = \begin{cases} 2\sqrt{-u_n^2 - u^2 + 1} & |u| < \sqrt{1-u_n^2} \\ 0 & else \end{cases} \tag{28}$$

$$\sigma_{\delta 3} = \begin{cases} 2uu_n \cos^{-1}\left(-\frac{uu_n}{\sqrt{1-u^2}\sqrt{1-u_n^2}}\right) - 2\pi u u_n \Theta(u u_n) & |u| < \sqrt{1-u_n^2} \\ 0 & else. \end{cases} \tag{29}$$

We can also compactly write

$$\sigma_\delta(u, u_n) = 2\mathrm{Re}\left(\sqrt{-u^2 - u_n^2 + 1} + u u_n \cos^{-1}\left(-\frac{u u_n}{\sqrt{1-u^2}\sqrt{1-u_n^2}}\right)\right). \tag{30}$$

This produces an interesting family of symmetric,

$$\sigma_\delta(a, b) = \sigma_\delta(b, a), \tag{31}$$

normalized,

$$\int_{-1}^{1} \sigma_\delta(u, u_n) \mathrm{d}u = \pi \tag{32}$$

functions (Figure 6). The Dirac cross section is closely related to a cross section for random plates in anisotropic random media studied in tree canopies (Nilson, 1968b,a; Myneni et al., 1988; Knyazikhin and Marshak, 1991). Similar expressions to Equation 26 appear in (Davison, 1957, p.235,Eq.(17.12)).

We can use the Dirac cross section as a Green's function and express the cross section of any symmetric normal distribution $D(u)$ as,

$$\sigma(u) = \int_{-1}^{1} \sigma_\delta(u, u') D(u') \mathrm{d}u'. \tag{33}$$

To acquire $\sigma(u)$ during rendering having only implemented $D(u)$, we numerically integrate Equation 33 using a Gaussian quadrature. To be conservative and non-adaptive, we chose 100 points, but fewer is likely sufficient in many cases, especially given the smooth NDF shapes likely to be efficient with the null-scattering algorithm.

3.3 Limitations

While the null-scattering approach for general microfacet BSDFs is very flexible, it has some important limitations. Highly-peaked (low roughness) NDFs will have very high rejection rates for almost all directions, not just upwelling ones, causing the method to perform poorly. In our experience, roughnesses below $\sigma = 0.4$ are not recommended.

Path tracing typically also requires a deterministic pdf() (if only approximate), in order to use MIS in a unidirectional path tracer, for example. For our tests using this method in Mitsuba 0.6 (Jakob, 2010), we used a Lambertian pdf in all cases. Given that the approach is best suited to highly rough materials (which have NDFs on the full sphere), we found that this compromise was adequate for an initial exploration of the space of biscale and porous BSDFs.

Both of these limitations leave open important areas for future work.

3.4 More NDFs

With the ease of adding new NDFs to the library, we note several additional parametric families that do not seem to have gained attention previously in rendering and might find use in some applications.

3.4.1 Bessel K NDF

We define a parametric NDF that interpolates the exponential (defined below) and Beckmann NDFs. Specifically, we define the Bessel K shape invariant NDF with roughness α and shape parameter $a > 0$ using continuous superpositions of Beckmanns to find

$$D^{\mathrm{K}}(u,\alpha,a) = \int_0^\infty \frac{e^{-\alpha'}\alpha'^{\gamma-2}}{\Gamma(\gamma-1)} D^{\mathrm{B}}\left(u,\alpha\sqrt{\alpha'}\right)\mathrm{d}\alpha' \tag{34}$$

$$= \int_0^\infty \frac{2^{1-a}e^{-\frac{\alpha'^2}{2}}\alpha'^{2a-1}}{\Gamma(a)} D^{\mathrm{B}}\left(u,\alpha\alpha'/\sqrt{2}\right)\mathrm{d}\alpha' \tag{35}$$

$$= \frac{2\left(1-u^2\right)^{\frac{a}{2}-\frac{1}{2}}(\alpha u)^{-a}K_{1-a}\left(\frac{2\sqrt{1-u^2}}{u\alpha}\right)}{\pi\alpha u^3\Gamma(a)} \tag{36}$$

where $K_v(x)$ is the Bessel-K function. The corresponding slope distribution is

$$P_{22}^{\mathrm{K}}(p,q,\alpha,a) = \frac{2\alpha^{-a-1}\left(p^2+q^2\right)^{\frac{a-1}{2}}K_{a-1}\left(\frac{2\sqrt{p^2+q^2}}{\alpha}\right)}{\pi\Gamma(a)} \tag{37}$$

with marginal slope distribution

$$P_2^{\mathrm{K}}(p,\alpha,a) = \frac{2\alpha^{-a-\frac{1}{2}}|p|^{a-\frac{1}{2}}K_{a-\frac{1}{2}}\left(\frac{2|p|}{\alpha}\right)}{\sqrt{\pi}\Gamma(a)}. \tag{38}$$

The Smith Λ function for the Bessel K NDF can be written

$$\Lambda^{\mathrm{K}}(u,\alpha,a) = \frac{u}{2} + \frac{\alpha^{-2a}\left(1-u^2\right)^{\frac{1}{4}-\frac{a}{2}}(\alpha u)^{a+\frac{1}{2}}K_{-a-\frac{1}{2}}\left(\frac{2u}{\sqrt{1-u^2}\alpha}\right)}{\sqrt{\pi}\Gamma(a)} +$$
$$\frac{1}{2}\sqrt{\pi}u\sec(\pi a)\left(\frac{\sqrt{\pi}u\,{}_1\tilde{F}_2\left(\frac{1}{2};\frac{3}{2},\frac{3}{2}-a;-\frac{u^2}{(u^2-1)\alpha^2}\right)}{\alpha\sqrt{1-u^2}\Gamma(a)} + \alpha^{-2a}u^{2a}\left(1-u^2\right)^{-a}\,{}_1\tilde{F}_2\left(a;a+\frac{1}{2},a+1;-\frac{u^2}{\left(u^2-1\right)\alpha^2}\right)\right). \tag{39}$$

For integer values of a, the Λ functions reduce to simpler expressions. For half-integer values of a, Meijer G functions appear (see BesselK.nb for more details).

As $a \to \infty$, the NDF $D^{\mathrm{K}}(u,\alpha/\sqrt{a},a)$ approaches the Beckmann NDF with roughness α (Bahar and Fitzwater, 1983). For $a = 3/2$, the Bessel K NDF reduces to the exponential NDF (below). Our definition is a generalization of a slope distribution proposed by Bahar and Fitzwater (1983) for integer values of a (to follow their constant-mean squared slope parameterization use $D^{\mathrm{K}}(u,\alpha/\sqrt{a},a)$).

The Bessel K_0 NDF ($a = 1$) For this value of a the resulting NDF is singular at $u = 1$ and has explicit Λ and cross section:

$$D^{\mathrm{K}}(u,\alpha,0) = \frac{2K_0\left(\frac{2\sqrt{1-u^2}}{u\alpha}\right)}{\pi\alpha^2u^4}\Theta(1-u) \tag{40}$$

$$\Lambda^{\mathrm{K}}(u,\alpha,0) = \frac{\alpha\sqrt{1-u^2}e^{-\frac{2u}{\alpha\sqrt{1-u^2}}}}{4u}, \quad 0 < u \le 1 \tag{41}$$

$$\sigma^{\mathrm{K}}(u,\alpha,0) = \frac{1}{4}\alpha\sqrt{1-u^2}\Theta(-u)e^{\frac{2u}{\alpha\sqrt{1-u^2}}} + u\Theta(u)\left(\frac{\alpha\sqrt{1-u^2}e^{-\frac{2u}{\alpha\sqrt{1-u^2}}}}{4u} + 1\right) \tag{42}$$

The K_0 NDF was also considered by Bourlier et al. (2002).

The Exponential NDF ($a = 3/2$) Microsufaces with an exponential distribution of slopes were proposed by several authors (Hughes, 1962; Muhleman, 1964; Hagfors, 1966; Barrick, 1968). Using a different parameterization of roughness, we define the the exponential shape invariant NDF to be

$$D^{\mathrm{Exp}}(u,\alpha) = \int_0^\infty \frac{2e^{-\alpha'}\sqrt{\alpha'}}{\sqrt{\pi}}D^{\mathrm{B}}(u,\alpha\sqrt{\alpha'})\mathrm{d}\alpha' = \frac{2e^{-\frac{2\sqrt{1-u^2}}{\alpha u}}}{\pi\alpha^2u^4}\Theta(1-u). \tag{43}$$

The corresponding slope distribution is

$$P_{22}^{\mathrm{Exp}}(p,q,\alpha) = \frac{2e^{-\frac{2\sqrt{p^2+q^2}}{\alpha}}}{\pi\alpha^2} \tag{44}$$

with marginal slope distribution

$$P_{2}^{\mathrm{Exp}}(p,\alpha) = \frac{4|p|K_1\left(\frac{2|p|}{\alpha}\right)}{\pi\alpha^2}. \tag{45}$$

The Smith Λ function for the Exponential NDF can be written

$$\Lambda^{\mathrm{Exp}}(u,\alpha) = \frac{G_{1,3}^{2,1}\left(\frac{u^2}{(1-u^2)\alpha^2}\middle|\begin{matrix}1\\ \frac{1}{2},\frac{3}{2},0\end{matrix}\right)}{\pi} + \frac{2uK_2\left(\frac{2u}{\sqrt{1-u^2}\alpha}\right)}{\pi\alpha\sqrt{1-u^2}} - \frac{1}{2} \tag{46}$$

in terms of Meijer G functions, which has an equivalent representation using Struve L functions Brown (1980). Bourlier et al. (2002) also considered Smith shadowing functions for exponential distributions of slopes. For accurate approximations of the Exponential NDF Lambda function, see Mathematica source code at: ExponentialNDF.nb.

4 Facet Forge

In the supplemental codebase facet-forge, we provide a C++ implementation of the above BSDF tools using a new object-oriented interface that minimizes the amount of code required to add a new NDF. By deriving from a common base NDF class, both a ShapeInvariantNDF and a NullNDF are implemented in such a way that the Microsurface class can operate with both through a common interface. The random walks required to implement unbiased multiple scattering from the microsurface are implemented only once (each for eval() and sample()), regardless of NDF and microfacet material type.

One benefit of this approach is that the Microsurface class is an operator that takes as input an NDF and a microsurface BSDF and outputs (implements) a new BSDF. This avoids having to specialize the random walks for each material type. For example, instead of implementing a RoughDielectricBSDF material, one simply passes the desired NDF and microsurface BSDF to the Microsuface class:

```
DielectricBSDF micro_brdf;
StudentTNDF ndf(&micro_brdf, rough_x, rough_y, gamma);
Microsurface brdf(&ndf);
```

and then calls eval() and sample() with the two directions and iors on either side of the medium. Because the Microsurface is itself a BSDF, it can be passed into another Microsurface to model biscale roughness, etc. We have briefly explored this behaviour in the supplemental images, discussed in the next section.

Our code is a direct extension of the prior implementation of Heitz et al. (2016) for heightfields, and the major differences are in the combination of support for singular and general microfacet BSDFs in the same random walk together with the joint sampling of new heights and microfacet orientations (which is required by the Null algorithm).

(a) Beckmann 0.4 (b) Beckmann 1.0 (c) Beckmann 4.0

(d) vMF 0.4 (e) vMF 1.0 (f) vMF 4.0

Figure 7: Our Null-scattering formulation of rough surface scattering permits implementation of new microfacet BRDFs with full-sphere NDFs (in this case vMF) by implementing a single function: the NDF distribution itself. Both models are similar for low roughness, but we see the porous model transition naturally into high roughness regimes without the unnatural sheen appearance that Beckmann suffers as all of the microfacets are constrained to the upper hemisphere.

5 Results

5.1 Biscale Roughness

In the supplemental images directory we provide a series of renders comparing biscale rough gold with Beckmann NDFs and identical roughnesses at each scale to a single-scale Beckmann roughness with an appropriately-scaled roughness to attempt an approximate match. We note that the biscale results have a less fuzzy/sheeny appearance, and that the difference is visible for surprisingly small roughness values.

5.2 Student-T Conductors and Diffuse Surfaces with Multiple Scattering

With an exact vNDF sampling for the Student-T NDF we computed (possibly the first) renders of rough conductors and diffuse surfaces with full multiple scattering. See the supplemental images folder to browse through the results over roughness and shape parameter and to compare the additional energy gained by including multiple scattering.

5.3 Porous Rough Gold using the vMF NDF

We implemented a NullNDF implementation of a spherical Gaussian (von-Mises-Fischer/vMF) NDF with roughness parameter α chosen to match Beckmann at low values, by implementing D as:

```
virtual double D(const Vector3& wm) const
{
    const double u = wm.z;
    return exp((2.0 * (-1.0 + u)) / (m_roughness*m_roughness));
};
```

No additional code is required and we can now render porous rough gold materials, etc. by passing whatever microfacet BSDF we like into the NDF class and then into the Microsurface class. We compare rough gold renders for three roughness values $\{0.4, 1.0, 4.0\}$ for Beckmann and vMF NDFs in Figure 7. Note how the Beckmann NDF unnaturally forces most facets to the vertical orientation for very high roughness values creating a bright sheen look, whereas the full-sphere NDF appears rougher and darker in a natural way as light bounces around in porous regions many times, being repeatedly absorbed.

References

Bahar, E. and M. A. Fitzwater
1983. Shadowing by non-Gaussian rough surfaces for which decorrelation implies statistical independence. *Radio science*, 18(04):566–572. https://doi.org/10.1029/RS018i004p00566.

Barrick, D.
1968. Rough surface scattering based on the specular point theory. *IEEE Transactions on Antennas and Propagation*, 16(4):449–454. https://doi.org/10.1109/TAP.1968.1139220.

Blinn, J. F.
1977. Models of light reflection for computer synthesized pictures. *Proceedings of 4th annual conference on Computer graphics and interactive techniques*, Pp. 192–198. https://doi.org/10.1145/563858.563893.

Bourlier, C., G. Berginc, and J. Saillard
2002. One-and two-dimensional shadowing functions for any height and slope stationary uncorrelated surface in the monostatic and bistatic configurations. *IEEE Transactions on Antennas and Propagation*, 50(3):312–324. https://doi.org/10.1109/8.999622.

Brown, G.
1980. Shadowing by non-Gaussian random surfaces. *IEEE Transactions on Antennas and Propagation*, 28(6):788–790. https://doi.org/10.1109/TAP.1980.1142437.

Butler, J.
1954. Machine sampling from given probability distributions. In *Symposium on Monte Carlo Methods*, Pp. 249–264. Wiley.

Davison, B.
1957. *Neutron Transport Theory*. Oxford University Press.

d'Eon, E.
2016. The anisotropic cross-section for the spherical Gaussian medium. Technical report. http://www.eugenedeon.com/wp-content/uploads/2016/07/sgcross.pdf.

d'Eon, E.
2022. *A Hitchhiker's Guide to Multiple Scattering*, v.0.3.2 edition. Self Published. http://www.eugenedeon.com/hitchhikers.

Dupuy, J., E. Heitz, and E. d'Eon
2016. Additional progress towards the unification of microfacet and microflake theories. In *EGSR (EI&I)*, Pp. 55–63. https://doi.org/10.5555/3056507.3056519.

Everett, C. and E. Cashwell
1983. A third Monte Carlo sampler. Technical Report LA-9721-MS, Los Alamos National Lab, N. Mex.(USA). https://permalink.lanl.gov/object/tr?what=info:lanl-repo/lareport/LA-09721-MS.

Georgiev, I., Z. Misso, T. Hachisuka, D. Nowrouzezahrai, J. Křivánek, and W. Jarosz
2019. Integral formulations of volumetric transmittance. *ACM Transactions on Graphics (Proceedings of SIGGRAPH Asia)*, 38(6). https://doi.org/10/dffn.

Guo, Y., M. Hašan, and S. Zhao
2018. Position-free Monte Carlo simulation for arbitrary layered BSDFs. *ACM Transactions on Graphics (ToG)*, 37(6):1–14. https://doi.org/10.1145/3272127.3275053.

Hagfors, T.
1966. Relationship of geometric optics and autocorrelation approaches to the analysis of lunar and planetary radar. *Journal of Geophysical Research*, 71(2):379–383. https://doi.org/10.1029/JZ071i002p00379.

Heitz, E.
2014. Understanding the masking-shadowing function in microfacet-based BRDFs. *Journal of Computer Graphics Techniques*, 3(2):32–91. http://jcgt.org/published/0003/02/03/.

Heitz, E. and E. d'Eon
2014. Importance sampling microfacet-based BSDFs using the distribution of visible normals. In *Computer Graphics Forum*, volume 33, Pp. 103–112. Wiley Online Library. https://doi.org/10.1111/cgf.12417.

Heitz, E., J. Hanika, E. d'Eon, and C. Dachsbacher
2016. Multiple-scattering microfacet BSDFs with the Smith model. *ACM Transactions on Graphics (TOG)*, 35(4):58. https://doi.org/10.1145/2897824.2925943.

Hughes, V.
1962. Diffraction theory applied to radio wave scattering from the lunar surface. *Proceedings of the Physical Society (1958-1967)*, 80(5):1117. https://doi.org/10.1088/0370-1328/80/5/311.

Jakob, W.
2010. Mitsuba renderer. http://www.mitsuba-renderer.org.

Jakob, W., A. Arbree, J. Moon, K. Bala, and S. Marschner
2010. A radiative transfer framework for rendering materials with anisotropic structure. *ACM Transactions on Graphics (TOG)*, 29(4):1–13. https://doi.org/10.1145/1778765.1778790.

Knyazikhin, Y. and A. Marshak
1991. Fundamental equations of radiative transfer in leaf canopies, and iterative methods for their solution. In *Photon-vegetation interactions*, Pp. 9–43. Springer. https://doi.org/10.1007/978-3-642-75389-3_2.

Muhleman, D.
1964. Symposium on radar and radiometric observations of Venus during the 1962 conjunction: Radar scattering from Venus and the Moon. *The Astronomical Journal*, 69:34. https://doi.org/10.1086/109225.

Myneni, R., V. Gutschick, G. Asrar, and E. Kanemasu
1988. Photon transport in vegetation canopies with anisotropic scattering Part III. Scattering phase functions in two angles. *Agricultural and forest meteorology*, 42(2-3):87–99. https://doi.org/10.1016/0168-1923(88)90070-6.

Nilson, T.
1968a. The calculation of spectral fluxes of shortwave radiation in plant communities. *Solar Radiation Regime in Plant Stand Acad Sci ESSR, Inst Phys Astron, Tartu, USSR*, Pp. 55–80.

Nilson, T.
1968b. On the optimum geometrical arrangement of foliage in the plant cover. *Solar Radiation Regime in Plant Stand Acad Sci ESSR, Institute of Physics and Astronautics, Tartu, USSR*, Pp. 112–146.

Novák, J., I. Georgiev, J. Hanika, and W. Jarosz
2018. Monte carlo methods for volumetric light transport simulation. In *Computer Graphics Forum*, volume 37, Pp. 551–576. Wiley Online Library. https://doi.org/10.1111/cgf.13383.

Ribardière, M., B. Bringier, D. Meneveaux, and L. Simonot
2017. STD: Student's t-Distribution of Slopes for Microfacet Based BSDFs. In *Computer Graphics Forum*, volume 36, Pp. 421–429. Wiley Online Library. https://doi.org/10.1111/cgf.13137.

Smith, B.
1967. Geometrical shadowing of a random rough surface. *IEEE transactions on antennas and propagation*, 15(5):668–671. https://doi.org/10.1109/TAP.1967.1138991.

Tadikamalla, P. R.
1979. Random sampling from the generalized gamma distribution. *Computing*, 23(2):199–203. https://doi.org/10.1007/BF02252098.

Walter, B., S. Marschner, H. Li, and K. Torrance
2007. Microfacet models for refraction through rough surfaces. In *Rendering Techniques (Proc. EG Symposium on Rendering)*, Pp. 195–206. Citeseer. http://dx.doi.org/10.2312/EGWR/EGSR07/195-206.